Universal measurement-based quantum computation in two-dimensional symmetry-protected topological phases

Tzu-Chieh Wei and Ching-Yu Huang

Universal measurement-based quantum computation in two-dimensional SPT phases

Tzu-Chieh Wei[1] and Ching-Yu Huang[1, 2]

[1] *C. N. Yang Institute for Theoretical Physics and Department of Physics and Astronomy,*
State University of New York at Stony Brook, Stony Brook, NY 11794-3840, USA
[2] *Physics Division, National Center for Theoretical Science, Hsinchu 30013, Taiwan*
(Dated: August 28, 2017)

Recent progress in characterization for gapped quantum phases has also triggered the search of universal resource for quantum computation in symmetric gapped phases. Prior works in one dimension suggest that it is a feature more common than previously thought in that nontrivial 1D symmetry-protected topological (SPT) phases provide quantum computational power characterized by the algebraic structure defining these phases. Progress in two and higher dimensions so far has been limited to special fixed points. Here we provide two families of 2D Z_2 symmetric wave functions such that there exists a finite region of the parameter in the SPT phases that supports universal quantum computation. The quantum computational power appears to lose its universality at the boundary between the SPT and symmetry-breaking phases.

I. INTRODUCTION AND MOTIVATION

Quantum mechanics allows certain computational tasks to be performed much more efficiently than using classical rules. The most celebrated example is the factoring of a large integer by Shor's quantum algorithm [1] that offers exponential speedup over existing classical algorithms, among many quantum algorithms showing superiority over classical counterparts [2–9]. Quantum computers that implement generic quantum algorithms can take various forms, such as the standard circuit model [10], the topological architecture [11], the adiabatic quantum computation [12, 13], and the quantum walk framework [14]. All these proceed via the unitary evolution of quantum mechanics, before the result is read out by measurement.

In contrast, the paradigm of the measurement-based quantum computation (MBQC) [15–17], with the teleportation-based schemes [18, 19] and the one-way quantum computer [15, 16, 20–22] as the prominent examples, offers an alternative framework, in which local measurement alone achieves the same power of computation as other models, provided that a prior sufficiently entangled state is given. One of the challenges in MBQC is to identify these entangled states, namely, the universal resource states that enable the success of driving universal quantum computation. It is known that states with too little entanglement, naturally, cannot provide sufficient quantum correlation to drive universal quantum computation [23, 24]. However, if a state possesses too much entanglement, the measurement outcome is so random that cannot provide any advantage over classical random guessing [25, 26]. Thus, it is the structure of the entanglement rather than its amount that is important for computation.

An intriguing connection of MBQC to condensed-matter physics emerges in the recent discovery of the symmetry-protected topological (SPT) phases [27–32], where states possess certain types of short-range entanglement. This connection was first revealed in the 1D SPT phase [33], where the SPT order can be utilized for the protection of certain quantum gates in MBQC, even though 1D quantum states do not naturally accommodate universal quantum computation. Examples include the 1D cluster state and the 1D spin-1 AKLT state, which can be used for arbitrary single-qubit gates [34, 35]. Such utility in quantum gates has been further explored [36] and holds in the entire SPT phases [37–39].

However, the development in two dimensions and higher is far limited, with only a handful of fixed-point wave functions providing universal resources [40–42], and the usefulness in some cases may depend on the underlying lattices. An important question remains open is whether the quantum computational universality can be extended beyond the fixed points in two or high-dimensional SPT phases. Here we consider two specific families of 2D symmetric wave functions and show that there exists a finite region in the parameter space that supports universal quantum computation. Such existence does not depend on lattices, even though the specific range of parameters does. The quantum computational power in the two families diminishes at the boundary between the SPT and symmetry-breaking phases. This shows positively that quantum computational universality is a feature beyond just the fixed point and is strongly related to the SPT order. (We remark that the universality used in this paper refers to quantum computation rather than the universality class in phase transitions.)

II. FAMILIES OF Z_2 SYMMETRIC WAVE FUNCTIONS: SPT AND SYMMETRY-BREAKING PHASES

We construct two families of Z_2 symmetric wave functions on the honeycomb and square lattices, respectively. Each physical site contains multiple qubits and each qubit forms part of a GHZ loop, $|00\ldots0\rangle + |11\ldots1\rangle$, with other qubits on a face. These loops form the ground state of the so-called CZX model [43], but we generalize the
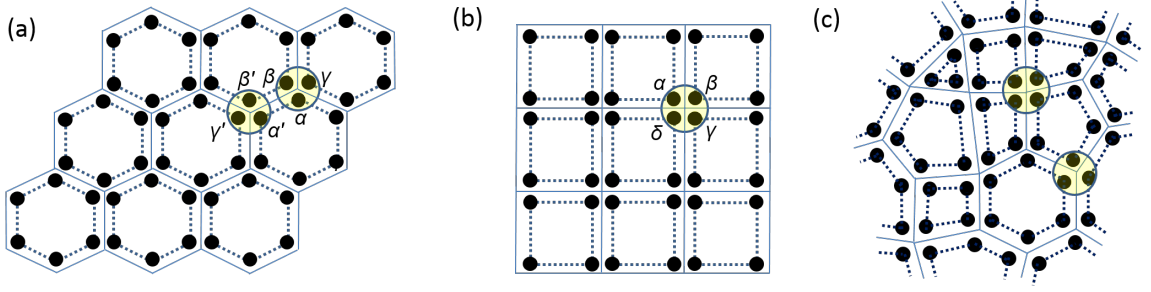
FIG. 1. Lattice and qubits: the each physical site (illustrated by a shaded circle) contains multiple qubits: three on (a) the honeycomb lattce, four on (b) the square lattice, and either three or four on (c) a random planar graph of mixed degrees 3 and 4. Each dashed loop indicates the constraint on the state of qubits connected by the loop; they need to the same either all $|0\rangle$ or all $|1\rangle$, i.e. a GHZ constraint: $|00\ldots0\rangle + |11\ldots1\rangle$.

construction beyond this fixed-point model. Our wave functions can be regarded as deformation from these exact GHZ loops and the weight of deformation (denoted by A) depends on the spin configurations on each site. Referring to Fig. 1 for the arguments of the tensor A, we have on the honeycomb lattice (previously studied by us [44]):

$$A(0,0,0) = A(1,1,1) = 1$$
$$A(0,0,1) = A(0,1,0) = A(1,0,0) = |g|$$
$$A(1,1,0) = A(1,0,1) = A(0,1,1) = g, \qquad (1)$$

and on the square lattice:

$$A[0,0,0,0] = A[1,1,1,1] = 1 \qquad (2)$$
$$A[0,0,1,1] = A[1,0,0,1] = g$$
$$A[1,1,0,0] = A[0,1,1,0] = A[0,1,0,1] = A[1,0,1,0] = |g|$$
$$A[0,0,1,0] = A[1,1,0,1] = A[1,0,0,0] = A[0,1,1,1] = |g|$$
$$A[0,1,0,0] = A[0,0,0,1] = A[1,0,1,1] = A[1,1,1,0] = |g|.$$

As one can see that under the local Z_2 action $\hat{u} = \sigma_x \otimes \cdots \otimes \sigma_x$, these weights display a symmetry, up to a possible sign (if $g < 0$), showing that the wave functions are symmetric under the action of the simple Z_2 group $G = \{\mathbb{1}, \hat{u}\}$; see also Appendix A. Short-range gapped parent Hamiltonians can be constructed such that these wave functions are the ground states [44].

Inspired by the works of Levin and Gu and of Hung and Wen [45, 46], we developed a tensor-network method (referred to as tnST) to probe the SPT phases by using the simulated modular matrices S and T [44], which originate from the duality between SPT and intrinsic topological order. Such a tnST method can distinguish nontrivial SPT order from trivial SPT order and spontaneous symmetry breaking by examining modular matrices. Essentially for the Z_2 symmetry, only the trace of T^2 is needed for the characterization of the SPT order [46], and we show the results in Fig. 2 that depict several distinct phases. These two families of wave functions display a common feature in the phase diagram: for the parameter g sufficiently negative, it is a nontrivial SPT
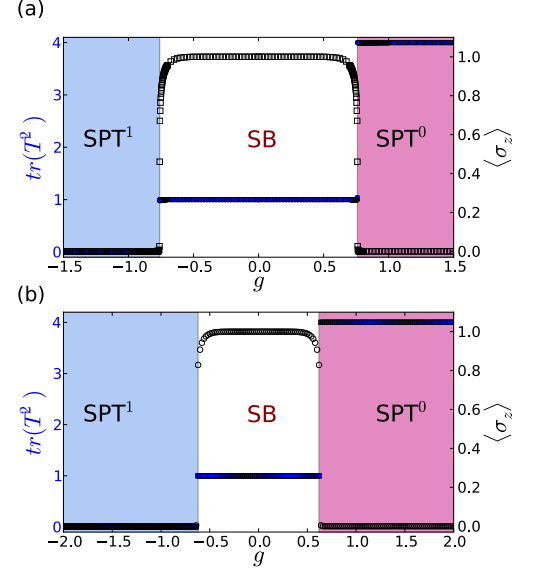

FIG. 2. Phase diagram vs. g. $\mathrm{Tr}(T^2)$ is represented by black empty squares and the order parameter $\langle\sigma_z\rangle$ is represented by blue empty circles. (a) Top panel: honeycomb lattice (see also Ref. [44]); (b) bottom panel: square lattice. The transitions are estimated to be at $|g_c| = 0.759(1)$ on the honeycomb lattice and at $|g_c| = 0.633(1)$ for the square lattice.

phase (labeled as SPT^1), and as g increases, there is a transition to a Z_2 spontaneous symmetry-breaking phase (labeled as SB), followed by another transition to a trivial SPT phase (labeled as SPT^0). The detailed forms of modular matrices are unitarily equivalent to those of the toric code (for SPT^1) and of the double semion (for SPT^1) [45, 46], and have just one diagonal element with unity (for SB), respectively; see also Appendix B. In the symmetry-breaking phase, the local order parameter is $\langle\sigma_z\rangle$ and it vanishes at the same boundaries obtained from $\mathrm{tr}(T^2)$.

III. UNIVERSAL QUANTUM COMPUTATION IN SPT PHASES

One of us has previously shown that universal quantum computation can be done using fixed-point nontrivial SPT states of Chen, Gu, Liu and Wen [32] on any 2D lattices [40]. Miller and Miyake also provide examples of Z_2^3 SPT-symmetric fixed-point wave function on the union-jack lattice [41, 42]. But an important question remains unanswered as to whether there exists an extended region (if not the whole phase) in an SPT phase that supports universal MBQC. As we shall see the two families of symmetric wave functions provide an affirmative answer; indeed, in a finite region of the parameter g, universal quantum computation is supported. To do this, we will construct local generalized measurement (i.e. POVM) so that we can convert the deformed wave function back to a fixed point, albeit the effective lattice structure (for which the GHZ loops are concerned) is modified. By indentifying the range of g such that the number of GHZ loops is macroscopic and no macroscopic size of GHZ loops, we can narrow down the quantum computational universality region. Moreover, we find that as one approaches the symmetry-breaking phase from the SPT side (either nontrivial or trivial), the universal quantum computational capability appears to diminish at the transition.

For simplicity we will focus on the honeycomb case, but our results also hold for the square case, except that the range of universality is different. Since the sign of g is local to each site of three qubits, for the purpose of quantum computation we can transform it away by a local unitary (or equivalently a local basis change):

$$U(g) = |000\rangle\langle000| + |111\rangle\langle111| \qquad (3)$$
$$+ |001\rangle\langle001| + |010\rangle\langle010| + |100\rangle\langle100|$$
$$+ \text{sgn}(g)(|110\rangle\langle110| + |101\rangle\langle101| + |011\rangle\langle011|),$$

where $\text{sgn}(g)$ is the sign function, which we take to be 1 if $g \geq 0$, and -1 if $g < 0$. Therefore, it suffices to take $g \geq 0$ and divide our consideration to two cases: (i) $g \leq 1$ and (ii) $g > 1$ and our results will hold for $g < 0$, too.

A. Case $g \leq 1$. We construct a local generalized measurement (i.e. POVM) that contains two elements $\{E_1 = F_1^\dagger F_1, E_2 = F_2^\dagger F_2\}$, where

$$F_1 = g(|000\rangle\langle000| + |111\rangle\langle111|)$$
$$+ |001\rangle\langle001| + |010\rangle\langle010| + |100\rangle\langle100|$$
$$+ |110\rangle\langle110| + |101\rangle\langle101| + |011\rangle\langle011|, \qquad (4)$$
$$F_2 = \sqrt{1 - g^2}(|000\rangle\langle000| + |111\rangle\langle111|). \qquad (5)$$

One can verify that $E_1 + E_2 = \mathbb{1}$ and thus the POVM is trace-preserving. The meaning of this POVM is as follows. Depending on the outcome $i = 1$ or 2, an initial state $|\psi\rangle$ is mapped to $F_i|\psi\rangle$ after the measurement. When the outcome is E_1, the local tensor is reduced back to the fixed-point form, except for a g factor:
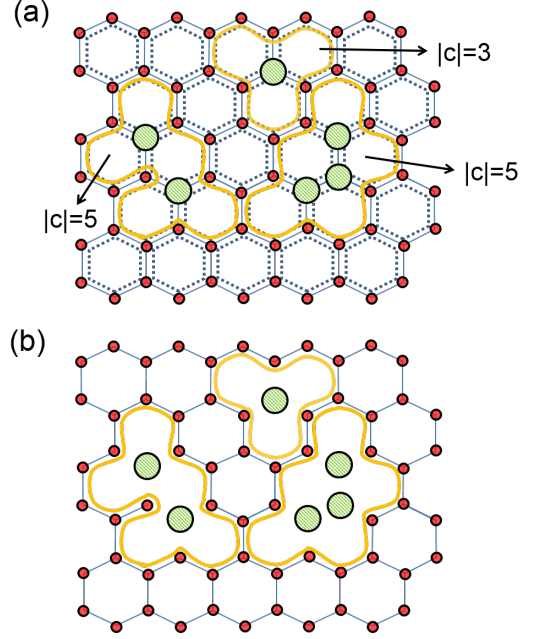

FIG. 3. Illustration of POVM outomes and GHZ loops. Solid green (larger, meshed) dots represent outcomes of E_2, while smaller red dots represent E_1 outcomes. Individual qubits are not shown. (a) A cluster is defined as a loop composed of one or multiple hexagons, with the latter indicated by a curved loop. (b) A simplified rendition of (a).

$A(\alpha, \beta, \gamma) = g$. When the outcome is E_2, the local tensor becomes

$$A(0,0,0) = A(1,1,1) = \sqrt{1 - g^2}, \ A(\text{rest}) = 0, \qquad (6)$$

where 'rest' indicates all other configurations than $(0,0,0)$ and $(1,1,1)$. Thus, the E_2 outcome results in the merging of the three GHZ loops surrounding the vertex into one giant loop; see Fig. 3. All qubits on and enclosed by the giant loop together form a GHZ state.

We label the POVM outcome by $\{\alpha_v\}$, where v denote a site and α_v can be either 1 (desired) or 2 (undesired). We label the total number of outcome E_1 by n_1 and that of E_2 by n_2, as well as the size of cluster c of loops by $|c|$ that counts the number of hexagons in a GHZ loop (see Fig. 3). An initial state $|\psi\rangle$ is transformed by the measurement to $\otimes_v F_{\alpha_v}|\psi\rangle$, and the probability that $\{\alpha_v\}$ occurs is

$$P_{\{\alpha_v\}}(g) = \frac{\langle\psi(g)| \otimes_v E_{\alpha_v}|\psi(g)\rangle}{\langle\psi(g)|\psi(g)\rangle} = \frac{\left\|\otimes_v F_{\alpha_v}|\psi\rangle\right\|^2}{\langle\psi(g)|\psi(g)\rangle}. \qquad (7)$$

The effect of POVM is to reduce the states to product of GHZ loops, and using this viewpoint we can show that

$$P_{\{\alpha_v\}}(g) = p_0 \, g^{2n_1}(1 - g^2)^{n_2} \, 2^{\sum_c (1-|c|)}, \qquad (8)$$

where p_0 is an overall constant independent of $\{\alpha_v\}$; see also Appendix C 1. The factor g^{2n_1} is due to the effect of F_1 and $(1 - g^2)^{n_2}$ is due to F_2 giving an overall
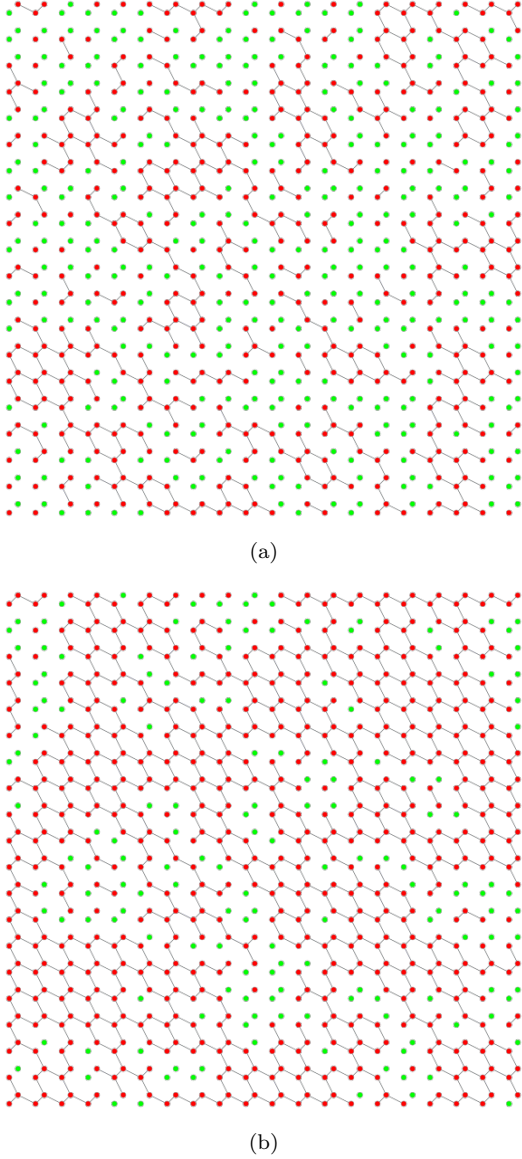
(a)

(b)

FIG. 4. Illustration of POVM outomes of a honeycomb lattice of 800 hexagons; (a) top panel: $g = 0.74$ (a macroscopic loops) and (b) bottom panel: $g = 0.78$ (no macroscopic loops). Loops are suppressed and E_1 outcomes are indicated by red dots (darker shades) and E_2 outcomes by green dots (lighter shades). But existence of a macrosopic loop can be seen from the existence of a pathway (like in a maze) from the left side to the right one or from the top to the bottom in (a).

$\sqrt{1 - g^2}$ factor. The factor $2^{\sum_c (1 - |c|)}$ arises due to the merging of loops by the action of F_2. With Eq. (8), we can employ the standard Monte Carlo method (see also Appendix D) to efficiently sample important configurations $\{\alpha_v\}$ for statistical analysis of, e.g., graph properties. From each outcome configuration, as illustrated in Fig. 4, we examine whether an undesired macroscopic loop may exist, using a percolation approach for probing the probability of such a spanning loop. As shown
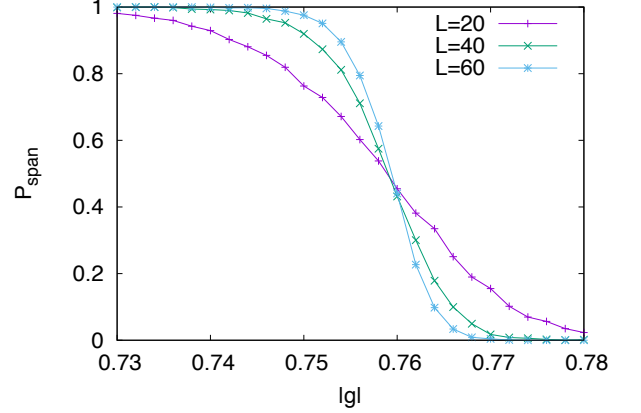

FIG. 5. Probability $P_{\rm span}$ of a spanning loop (i.e. a macroscopic GHZ loop) vs. parameter g for the case $g < 1$ for various linear sizes L on the honeycomb lattice. The total number of hexagons is $2L^2$. Each data point is averaged over 2000-4000 samples and the statistical error is less than 1%. A percolation transition is estimated at $g_{c1} \approx 0.760(2)$ in the thermodynamic limit. In the region $g_{c1} < g \leq 1$, there is no macroscopic GHZ loop ($P_{\rm span} \to 0$ as $L \to \infty$) and hence a sufficiently large valence-bond state with the number of qubits being proportional to the original system size can be obtained. This means that the system provides a universal resource for MBQC.

in Fig. 5, for $g > g_{c1} \approx 0.760(2)$, no such spanning loop exists in the thermodynamic limit, and thus there will be macroscopic number of small loops that can be further converted by additional local measurements to a valence-bond state which is universal [19, 40]. We find that the location of $g_{c1} \approx 0.760(2)$ to be very close, if not identical, to the transition from the SPT phase to the Z_2 symmetry-breaking phase. This is due to the emergence of long-range order as g approaches g_{c1}.

B. Case $g > 1$. In this region, we need to employ a different trace-perserving POVM that contains two elements $\{E_3 = F_3^\dagger F_3, E_4 = F_4^\dagger F_4\}$, where

$$F_3 = \frac{1}{g}(|001\rangle\langle 001| + |010\rangle\langle 010| + |100\rangle\langle 100|$$
$$+ |110\rangle\langle 110| + |101\rangle\langle 101| + |011\rangle\langle 011|) \tag{9}$$
$$+ (|000\rangle\langle 000| + |111\rangle\langle 111|) \tag{10}$$

$$F_4 = \frac{\sqrt{g^2 - 1}}{g}(|001\rangle\langle 001| + |010\rangle\langle 010| + |100\rangle\langle 100|$$
$$+ |110\rangle\langle 110| + |101\rangle\langle 101| + |011\rangle\langle 011|). \tag{11}$$

When the outcome is E_3, the local tensor is reduced back to the fixed-point form, except for the $1/g$ factor. When the outcome is E_4, the local tensor becomes

$$A(0,0,0) = A(1,1,1) = 0, \quad A(\text{rest}) = \sqrt{g^2 - 1}, \tag{12}$$

and this means that the three GHZ loops surrounding the

vertex have been merged into one giant loop of a generalized GHZ state that can have more than two components. For example, one single site with E_4 outcomes merged the three neighboring hexagon loops of GHZ states into one GHZ state of six components

$$
\begin{aligned}
&|0...0\rangle|0...0\rangle|1...1\rangle + |1...1\rangle|1...1\rangle|0...0\rangle \\
&+ |0...0\rangle|1...1\rangle|0...0\rangle + |1...1\rangle|0...0\rangle|1...1\rangle \\
&+ |1...1\rangle|0...0\rangle|0...0\rangle + |0...0\rangle|1...1\rangle|1...1\rangle.
\end{aligned} \quad (13)
$$

To recover the case of two-component GHZ state, one can follow up with a local measurement that consists of four projections at the vertex (after the E_4 outcome): $P_0 = |000\rangle\langle000| + |111\rangle\langle111|$, $P_1 = |001\rangle\langle001| + |110\rangle\langle110|$, $P_2 = |010\rangle\langle010| + |101\rangle\langle101|$, $P_3 = |100\rangle\langle100| + |011\rangle\langle011|$. There will not be a result associated with P_0, and each outcome associated with either P_1, P_2 or P_3, projects the local Hibert space to a two-level subspace that can be locally converted to the P_0 subspace. The reduction to a universal resource state then goes as before.

We use a similar labeling here of the POVM outcome by $\{\alpha_v\}$, except that α_v can be either 3 (desired) or 4 (undesired), and the total number of outcome E_3 by n_3 and that of E_4 by n_4. Similar to $g < 1$ case, we have (see also Appendix C 2)

$$
P_{\{\alpha_v\}} = p_0' \, g^{-2n_3} \left(\frac{g^2 - 1}{g^2} \right)^{-n_4} \prod_c q_c \, 2^{-|c|}, \quad (14)
$$

where p_0' is an overall constant that is independent of $\{\alpha_v\}$, and q_c counts the number of components in the merged generalized GHZ state for the cluster c. For the previous $g < 1$ case, the $q_c = 2$, but due to the more complicated structure in the E_4, here, q_c can be larger than 2. We do not know of any exact expression for q_c but we can bound the q_c by $6 \leq q_c \leq 6^{|c|/3}$, and these can be used in Monte Carlo simulations similar to that in Fig. 5 to find the bounds of the corresponding transition point g_{c2}, for which we obtain $1.205(5) \lesssim g_{c2} \lesssim 1.390(2)$.

However, there is no transition of phases nearby. There are two possibilities: one being that our POVM for $g > 1$ is not optimal but the quantum computational power extends further beyond, or it is possible that the quantum computational power does not extend all the way to the whole SPT phase. However, at the present we do not have a means to resolve this.

C. Square lattice. For the Z_2 symmetric wave functions on the square lattice, we repeat a similar procedure and obtain that there also exists a finite region in the SPT phases: $g_{c1} < |g| < g_{c2}$ supporting universal quantum computation, and we estimate that $g_{c1} \approx 0.635(3)$ and $1.31(1) \lesssim g_{c2} \lesssim 1.82(1)$; see Appendix E.

D. Breaking translational invariance. The construction above can be straightforwardly extended to other trivalent lattices, such as the square octagon, cross and star lattices and other four-valent lattices, such as the kagome lattice, and the probablility distribution of the POVM outcomes will be of similar forms. At $|g| = 1$

the wave functions are the fixed-point ones and thus the quantum computational universality is guaranteed [40]. Away from $|g| = 1$, the probability of undesired POVM outcomes, such as E_2 or E_4, is small so there will be a finite region around $|g| = 1$ such that the universality persists. The range of g can be found using methods described here but depends on the lattice and is a generalized percolation problem. To break the translational invariance, we can consider random planar graphs with vertex degrees being three or four or even of mixed degree (see Fig. 1c) and construct the family of wave functions in a similar way. As long as these graphs reside in the supercritical phase of percolation, the fixed point $|g| = 1$ possesses quantum computational universality. Away from $|g| = 1$ as in the uniform case, there is a finite region around it such that the universality is perserved. Thus our results of a finite region in the Z_2 SPT phase with quantum computational universality do not rely on translation invariance.

IV. DISCUSSIONS

We have constructed families of Z_2 symmetric wave functions and identified three distinct phases using modular matrices. For an extended region in the SPT phases, we have shown that universal quantum computation is possible via local measurements. Our construction can be straightforwardly extended to the non-translation invariant case. Previous quantum computational universality was only known for certain SPT fixed-point wave functions and may also depend on the lattice. Our results go beyond those and strengthen the potential connection of SPT order and quantum computation, which has been much explored in one dimension.

From the viewpoint of SPT order and higher dimensionality, the only exception so far is the family of AKLT states in two and higher dimensions [47–52] and many of them have been shown to provide universal resource for quantum computation even beyond the AKLT points [53–55]. But their SPT order requires translation invariant symmetry to be respected. For our Z_2 symmetric wave functions, the existence of SPT order and the quantum computational universality do not require translation invariance and is of one-dimensional nature.

It may seem puzzling why both the trivial and nontrivial SPT phases in our construction share similar quantum computational capability. This is because of our choice of symmetry group that protects the phase. To claim a state to be in an SPT phase, we need to specify the symmetry group. Even though our $g > 0$ families of states belong to a trivial Z_2 SPT phase with respect to the simple Z_2 group used here, they actually display nontrivial SPT order with respect to another Z_2 group generated by the so-called CZX action [43]. But then for the full-range of the parameter g the symmetry action depends on the sign of g, which is not a desirable feature. In our construction, the Z_2 action is the same across the whole

parameter range, and is simply a spin flip.

Our results can be extended to three dimensions. However, the fourth cohomology group of Z_2 is trivial, so to have a nontrivial SPT phases, we need to have the symmetry group larger than Z_2, such as $Z_2 \otimes Z_2$. Then the qubit in our Z_2 example needs to be replaced by a ququart, i.e. 4-level entity.

From a very different perspective, our results also imply that classical simulations of local measurements on the Z_2 SPT phases can be as hard as simulating outcome probability of a universal quantum computer, i.e. BQP. But on the other hand, simulating only the POVM outcomes of those constructed here (at least for $g \leq 1$), is easy, i.e. in P.

Appendix A: Z_2 symmetry of the wave functions

In this and the following sections, we supply detailed discussions of points that were mentioned in the main text, including (i) Symmetry of the wave functions; (ii) modular matrices; (iii) probability of POVM outcomes; and (iv) Monte Carlo simulations.

1. Honeycomb lattice

For convenience we reproduce the wave functions on the honeycomb lattice as follows,

$$A(0,0,0) = A(1,1,1) = 1$$
$$A(0,0,1) = A(0,1,0) = A(1,0,0) = |g|$$
$$A(1,1,0) = A(1,0,1) = A(0,1,1) = g. \quad (A1)$$

The wave functions can be represented by local tensors, as shown in Fig. 6(a), where the indices for the physical spin degree of freedom, e.g., α, is indentical to the two inner indices, a_1 and a_2, which originates from the constraint of an underlying GHZ entanglement. It is easy to verify that these wave functions are invariant under the $\mathbb{Z}_2$ action generated by the operator $X = \sigma_x = |0\rangle\langle 1| + |1\rangle\langle 0|$ (indicated on a boxed X next to each physical index) on all partons. However, the transformed tensors differ from the original ones by a local unitary transformation or local matrix-product operator (MPO) on the inner indices which is given by $X \otimes X\hat{O}$, as shown in Fig. 6(b), where

$$\hat{O} = |00\rangle\langle 00| + |01\rangle\langle 01| + \text{sgn}(g)|10\rangle\langle 10| + |11\rangle\langle 11|, \quad (A2)$$

and $\text{sgn}(g)$ is the sign function, which we take to be 1 if $g \geq 0$, and -1 if $g < 0$. This also gives a way of verifying that the wave function is $\mathbb{Z}_2$ symmetric, as the MPOs from neighboring sites cancel one another.

For such a fixed-point SPT wave function and others for nontrivial SPT phases, it was shown that they provide universal resource for quantum computation in the measurement-based model, where only local operations or measurements are needed to achieve universal quantum computation.

2. Square lattice

For convenience we reproduce the wave functions on the square lattice as follows,

$$A[0,0,0,0] = A[1,1,1,1] = 1 \quad (A3)$$
$$A[0,0,1,1] = A[1,0,0,1] = g$$
$$A[1,1,0,0] = A[0,1,1,0] = A[0,1,0,1] = A[1,0,1,0] = |g|$$
$$A[0,0,1,0] = A[1,1,0,1] = A[1,0,0,0] = A[0,1,1,1] = |g|$$
$$A[0,1,0,0] = A[0,0,0,1] = A[1,0,1,1] = A[1,1,1,0] = |g|.$$

Similar to the honeycomb case, the wave functions on the square lattice can be represented by local tensors, as shown in Fig. 7(a). It is easy to verify that these wave functions are invariant under the $\mathbb{Z}_2$ action generated by the operator $X = \sigma_x = |0\rangle\langle 1| + |1\rangle\langle 0|$ (indicated on a boxed X next to each physical index) on all partons. However, the transformed tensors differ from the original ones by a local unitary transformation or local matrix-product operator (MPO) on the inner indices which is given by $X \otimes X\hat{O}$, as shown in Fig. 7(b), where $\hat{O}$ differs slightly from that in the honeycomb case,

$$\hat{O} = |00\rangle\langle 00| + |01\rangle\langle 01| + |10\rangle\langle 10| + \text{sgn}(g)|11\rangle\langle 11|. \quad (A4)$$

This also gives a way of verifying that the wave function is $\mathbb{Z}_2$ symmetric, as the MPOs from neighboring sites cancel one another.

Appendix B: Z_2 SPT order and modular S and T matrices

Here we show the explict form of the modular S and T matrices from our numerical results.

1. Honeycomb case

When $-0.760(2) \leq g < 0.760(2)$, the modular matrices are

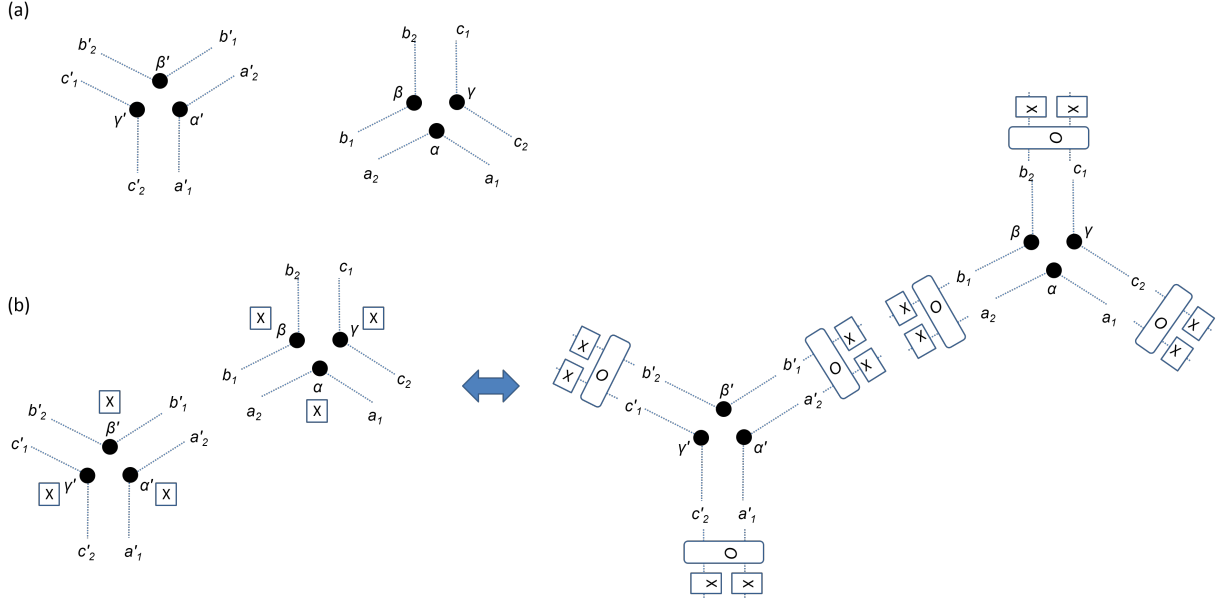$$S = T = \begin{pmatrix} 1 & 0 & 0 & 0 \\ 0 & 0 & 0 & 0 \\ 0 & 0 & 0 & 0 \\ 0 & 0 & 0 & 0 \end{pmatrix}, \quad (B1)$$

FIG. 6. (a) Local tensors for the wave functions. (b) The Z_2 symmetry action on the physical spins is equivalent to the local MPO action in the inner indices. In the drawing, operator $\hat{O}$ is applied first, followed by $X \otimes X$. But in the equation for the local MPO, one usually writes $\hat{O} X \otimes X$, reversing the order. As one can see that the neighboring local MPOs cancel and for a closed surface the wave functions are indeed Z_2 symmetric.

FIG. 7. (a) Local tensors for the wave functions. (b) The Z_2 symmetry action on the physical spins is equivalent to the local MPO action in the inner indices. In the drawing, operator $\hat{O}$ is applied first, followed by $X \otimes X$. But in the equation for the local MPO, one usually writes $\hat{O} X \otimes X$, reversing the order. As one can see that the neighboring local MPOs cancel and for a closed surface the wave functions are indeed Z_2 symmetric.

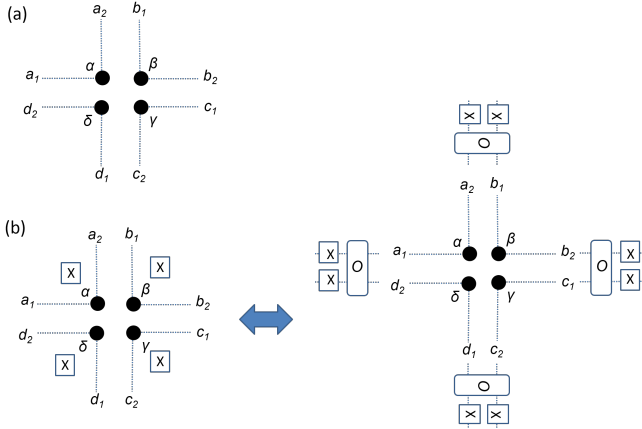and they show that it is a symmetry-breaking phase. When $g > 0.760(2)$, the modular matrices are

$$
S = \begin{pmatrix} 1 & 0 & 0 & 0 \\ 0 & 0 & 1 & 0 \\ 0 & 1 & 0 & 0 \\ 0 & 0 & 0 & 1 \end{pmatrix}, \quad T = \begin{pmatrix} 1 & 0 & 0 & 0 \\ 0 & 1 & 0 & 0 \\ 0 & 0 & 0 & 1 \\ 0 & 0 & 1 & 0 \end{pmatrix}. \quad (B2)
$$

One can diagonalize the T matrix and obtain the corresponding S matrix (also enforcing the elements in first row and the first column to be $1/2$)

$$
T' = \begin{pmatrix} 1 & 0 & 0 & 0 \\ 0 & 1 & 0 & 0 \\ 0 & 0 & 1 & 0 \\ 0 & 0 & 0 & -1 \end{pmatrix}, \quad (B3)
$$

$$
S' = \frac{1}{2}\begin{pmatrix} 1 & 1 & 1 & 1 \\ 1 & 1 & -1 & -1 \\ 1 & -1 & 1 & -1 \\ 1 & -1 & -1 & 1 \end{pmatrix}, \quad (B4)
$$

which are the modular matrices of the toric code. In this region, $\mathrm{Tr}(T^2) = 4$, showing the trivial $\mathbb{Z}_2$ SPT order (SPT^0). For $g < -0.760(2)$, the modular matrices are

$$
S = \begin{pmatrix} 1 & 0 & 0 & 0 \\ 0 & 0 & 1 & 0 \\ 0 & 1 & 0 & 0 \\ 0 & 0 & 0 & -1 \end{pmatrix}, \quad T = \begin{pmatrix} 1 & 0 & 0 & 0 \\ 0 & 1 & 0 & 0 \\ 0 & 0 & 0 & -1 \\ 0 & 0 & 1 & 0 \end{pmatrix}, \quad (B5)
$$

with $\mathrm{Tr}(T^2) = 0$. This shows a nontrivial $\mathbb{Z}_2$ SPT order (SPT^1). Similarly, we can diagonalize T and transform S to the same basis:

$$
T' = \begin{pmatrix} 1 & 0 & 0 & 0 \\ 0 & 1 & 0 & 0 \\ 0 & 0 & i & 0 \\ 0 & 0 & 0 & -i \end{pmatrix}, \quad S' = \frac{1}{2}\begin{pmatrix} 1 & 1 & 1 & 1 \\ 1 & 1 & -1 & -1 \\ 1 & -1 & -1 & 1 \\ 1 & -1 & 1 & -1 \end{pmatrix}, \quad (B6)
$$

which are the modular matrices for the double-semion model.

2. Square case

The modular matrices have the same forms in the respective symmetry-breaking, trivial SPT and nontrivial SPT phases. The only difference is the range of the parameter g.

Appendix C: Probability of a POVM outcome: the honeycomb lattice

Here we derive the probability for the POVM outcome, labelled by $\{\alpha_v\}$, on all sites of the honeycomb lattice.

1. Case $|g| \leq 1$

Since the phase is local to each site of three qubits, for the purpose of quantum computation we can transform it away by local unitary. We can apply a local unitary transformation on each site:

$$U(g) = |000\rangle\langle000| + |111\rangle\langle111| \tag{C1}$$
$$+|001\rangle\langle001| + |010\rangle\langle010| + |100\rangle\langle100|$$
$$+\text{sgn}(g)(|110\rangle\langle110| + |101\rangle\langle101| + |011\rangle\langle011|),$$

where $\text{sgn}(g)$ is the sign function, which we take to be 1 if $g \geq 0$, and -1 if $g < 0$. Thus, for simplicity, we only need to consider $g > 0$ case. For $0 \leq g \leq 1$, we construct a local POVM that contains two elements $\{E_1 = F_1^\dagger F_1, E_2 = F_2^\dagger F_2\}$, where

$$F_1 = g(|000\rangle\langle000| + |111\rangle\langle111|)$$
$$+|001\rangle\langle001| + |010\rangle\langle010| + |100\rangle\langle100|$$
$$+|110\rangle\langle110| + |101\rangle\langle101| + |011\rangle\langle011|, \tag{C2}$$
$$F_2 = \sqrt{1-g^2}(|000\rangle\langle000| + |111\rangle\langle111|). \tag{C3}$$

One can verify that $E_1 + E_2 = \mathbb{1}$ and thus the POVM is trace-preserving. When the outcome is E_1, the local tensor is reduced back to the fixed-point form, except for the g factor,

$$A(0,0,0) = A(1,1,1) = g,$$
$$A(0,0,1) = A(0,1,0) = A(1,0,0) = g$$
$$A(1,1,0) = A(1,0,1) = A(0,1,1) = g. \tag{C4}$$

When the outcome is E_2, the local tensor becomes

$$A(0,0,0) = A(1,1,1) = \sqrt{1-g^2},$$
$$A(0,0,1) = A(0,1,0) = A(1,0,0) = 0$$
$$A(1,1,0) = A(1,0,1) = A(0,1,1) = 0, \tag{C5}$$

and this means that the three GHZ loops surrounding the vertex have been merged into one giant loop.

We label the POVM outcome by $\{\alpha_v\}$, where v labels the site and α_v can be either 1 (desired) or 2 (undesired) measurement outcome. We label the total number of

outcome E_1 by n_1 and that of E_2 by n_2 and the size of cluster c by $|c|$. The latter $|c|$ counts the number of hexagons in a loop (see Fig. 3 of the main text). We can show that the probability of a particular outcome $\{\alpha_v\}$ is proportiontal to

$$P_{\{\alpha_v\}} = p_0\, g^{2n_1}(1-g^2)^{n_2}\, 2^{\sum_c(1-|c|)}, \tag{C6}$$

where p_0 is an overall constant that is independent of $\{\alpha_v\}$.

To see this, we first observe that the wave function at $g = 1$ corresponds to a product of (un-normalized) GHZ loops (with the number equal to the number of faces), i.e. each loop on a hexagon containing six qubits is in a state $|000000\rangle + |111111\rangle$. Away from this fixed point $g \neq 1$, the GHZ loops get distorted and become entangled through the local deformation at a vertex. The effect of E_1 at a vertex v is to restore locally so that the three qubits are disentangled and if all six vertices around a hexagon have E_1 outcome then the GHZ loop in that hexagon is restored. Each E_1 contributes a factor of g in the wave function. The effect of E_2 at site v is to merge the three GHZ loops passing this vertex and to multiply the wave function by a factor of $\sqrt{1-g^2}$. Therefore, for any configuration of outcomes at all sites $\{\alpha_v\}$, the resulting state is a product of GHZ loops, but their number is equal to $n_F - \sum_c(|c|-1)$, where n_F is the total number of faces or hexagons in the lattice. Each un-normalized GHZ loop contribute to a factor of 2 in the probability. Taking into account of n_1 factors of g and n_2 factors of $\sqrt{1-g^2}$ in the amplitude, we arrive at

$$P_{\{\alpha_v\}} = g^{2n_1}(1-g^2)^{n_2}\, 2^{\sum_c(1-|c|)}2^{n_F}/\langle\psi(g)|\psi(g)\rangle, \tag{C7}$$

where $\langle\psi(g)|\psi(g)\rangle$ is the norm square of the original un-normalized wave function, which can also be omitted for the purpose of Monte Carlo sampling, and the factor involing n_F can be omitted as well. Therefore, we have proved the expression in Eq. (C6).

We remark that Eq. (C6) can be interpreted as the Boltzmann weight of a statistical model of interacting particles of two types:

$$P_{\{\alpha_v\}}(g) \sim e^{-n_1\epsilon_1 - n_2\epsilon_2 - U_2}, \tag{C8}$$

where a type-1 particle costs energy $\epsilon_1 \equiv \ln(1/g^2)$ and a type-2 particle costs $\epsilon_2 \equiv \ln(1/(1-g^2))$, and additionally the interacton potential U_2 among type-2 particles due to loop stretching and merging: $-|c|\ln 2$, where $|c|$ depends on the configuration of the type-2 particles.

2. Case $|g| > 1$

In this region of the parameter, we consider a different POVM that contains two elements $\{E_3 = F_3^\dagger F_3, E_4 = $

$F_4^\dagger F_4\}$, where

$$F_3 = \frac{1}{g}(|001\rangle\langle001| + |010\rangle\langle010| + |100\rangle\langle100|$$
$$+|110\rangle\langle110| + |101\rangle\langle101| + |011\rangle\langle011|) \quad (C9)$$
$$+(|000\rangle\langle000| + |111\rangle\langle111|) \quad (C10)$$
$$F_4 = \frac{\sqrt{g^2-1}}{g}(|001\rangle\langle001| + |010\rangle\langle010| + |100\rangle\langle100|$$
$$+|110\rangle\langle110| + |101\rangle\langle101| + |011\rangle\langle011|). \quad (C11)$$

One can verify that $E_3 + E_4 = \mathbb{1}$ and thus the POVM is trace-preserving. When the outcome is E_3, the local tensor is reduced back to the fixed-point form, except for the $1/g$ factor. When the outcome is E_4, the local tensor becomes

$$A(0,0,0) = A(1,1,1) = 0,$$
$$A(0,0,1) = A(0,1,0) = A(1,0,0) = \sqrt{g^2-1}$$
$$A(1,1,0) = A(1,0,1) = A(0,1,1) = \sqrt{g^2-1}. \quad (C12)$$

and this means that the three GHZ loops surrounding the vertex have been merged into one giant loop that can have more than two components. For example, one single site with E_4 outcomes merged the three neighboring hexagon loops of GHZ state into one GHZ state of six components

$$|0...0\rangle|0...0\rangle|1...1\rangle + |1...1\rangle|1...1\rangle|0...0\rangle$$
$$+ |0...0\rangle|1...1\rangle|0...0\rangle + |1...1\rangle|0...0\rangle|1...1\rangle$$
$$+ |1...1\rangle|0...0\rangle|0...0\rangle + |0...0\rangle|1...1\rangle|1...1\rangle. \quad (C13)$$

To recover the case of two-component GHZ state, one can perform a measurement that consists of three projection at the vertex (after the E_2 outcome): $P_0 = |000\rangle\langle000| + |111\rangle\langle111|$, $P_1 = |001\rangle\langle001| + |110\rangle\langle110|$, $P_2 = |010\rangle\langle010| + |101\rangle\langle101|$, $P_3 = |100\rangle\langle100| + |011\rangle\langle011|$. Since the measurement is done following the E_2 outcome, there will not be an outcome associated with P_0, and each outcome associated with either P_1, P_2 or P_3, projects to a level-two subspace that can be locally converted to P_0 subspace. The reduction to a universal resource state goes as before, up to local rotation.

We label the POVM outcome similarly by $\{\alpha_v\}$, where v labels the site and α_v can be either 3 (desired) or 4 (undesired) measurement outcome. We also label the total number of outcome E_3 by n_3 and that of E_4 by n_4. We show below that the probability of a particular outcome $\{\alpha_v\}$ is proportiontal to

$$P_{\{\alpha_v\}} = p_0' \, g^{-2n_3} \left(\frac{g^2-1}{g^2}\right)^{-n_4} \prod_c q_c \, 2^{-|c|}, \quad (C14)$$

where p_0' is an overall constant that is independent of $\{\alpha_v\}$, and q_c counts the number of components in the merged generalized GHZ state for the cluster c. For the previous $g < 1$ case, the $q_c = 2$, but due to the more complicated structure in the E_4 here, q_c can be larger

than 2. But since there are 6 components in E_4, we have a lower bound $q_c \geq 6$. We also observe that $q_c \leq 6^{|c|/3}$, for which an example of saturation is $|c| = 3$ for a triangle.

The proof for Eq. (C14) is similiar to that of Eq. (C6). Since $g > 1$ we can divide the original tensor by this factor, and thus we turn the problem of $g > 1$ to $1/g < 1$. Thus the role of E_1 is now played by E_3 and that of E_2 by E_4, except that E_4 contains 6 rank-1 projectors, whereas E_2 contains 2 rank-1 projectors. The factor 2^1 in Eq. (C6) exactly counts the two components in the GHZ loop but now the loop will contain more components of at least 6. Thus we denote the total number of components in a loop inside a cluster c by q_c. This establishes the proof for Eq. (C14). We do not know of a closed form for q_c using simple geometric properties of the cluster, such as the number of its vertices, edges or loops. The counting has to be done case by case. Thus in our Monte Carlo simulations we will replace q_c by its bounds $6 \leq q_c \leq 6^{|c|/3}$, and at least the transition point of the quantum computational universality can be bounded.

We remark that the above analysis for the probability distribution extends to other lattices with appropriate extension of SPT wave functions, such as the square lattice or even 3D cubic or diamond lattices.

## Appendix D: Monte Carlo simulations for quantum computational universality

With the derived probability for any given outcome $\{\alpha_v\}$, we can employ Monte Carlo methods. In particular, we use the Metropolis method to attempt to flip at a site (labeled by zero) from E_1 to E_2 or vice versa for $g < 1$ (and between E_3 and E_4 for $g > 1$), denoted by $\alpha_0 \to \alpha_0'$. The probability ratio of $P_{\alpha_{v\neq0};\alpha_0'}/P_{\alpha_{v\neq0};\alpha_0}$ depends locally on Δn_1 and Δn_2, but quasi-locally on $|c|$ and $|c'|$. The cluster size can be obtained by a Wolff-like algorithm, and is the bottleneck of the simulations. The flip is accepted with a probability

$$P_{\text{accept}} = \min\{1, P_{\alpha_{v\neq0};\alpha_0'}/P_{\alpha_{v\neq0};\alpha_0}\}. \quad (D1)$$

The initialization of configuration $\{\alpha_v\}$ can be assigned randomly (i.e. hot start) or uniformly to E_1 or E_2 (cold start).

From the argument of continuity, we expect that there exist a $g_{c1} < 1$ and $g_{c2} > 1$ such that for $g \in (g_{c1}, g_{c2})$ inside the SPT phase, the quantum computation using the SPT ground states as the resource for MBQC is universal.

We find that the location of $g_{c1} \approx 0.760(2)$ to be very close, if not identical, to the transition from the SPT phase to the Z_2 symmetry breaking phase. It is likely that the transition in the quantum computational power coincides with the transition to the symmetry-breaking phase. This is due to the fact that the long-range order starts to form at the beginning of a percolated phase. This suggests that the POVM is optimal for $g < 1$. For the other side $g > 1$, we can bound the value of g_{c2}:
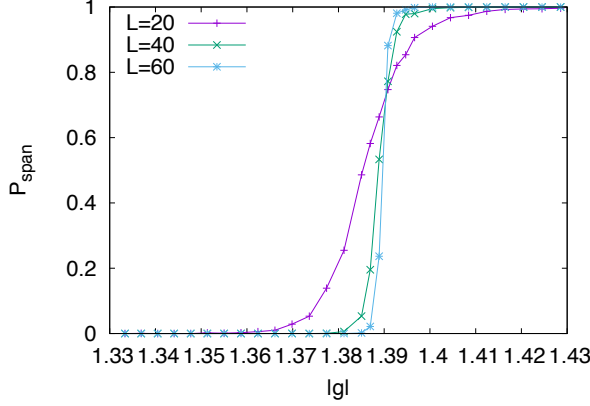
(a)
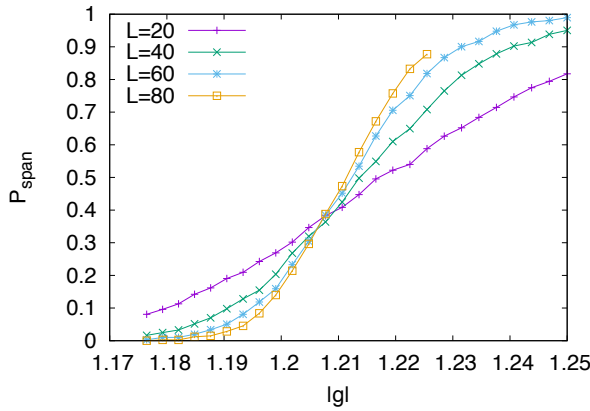
(b)

FIG. 8. Probability P_{span} of a spanning loop (i.e. a macroscopic GHZ loop) vs. parameter g for the case $g > 1$ on the honeycomb lattice. The top panel gives an estimate of the upper bound whereas the bottom panels gives the lower bound on the threshold value g_{c2} that separates regions with and without quantum computational universality. It is estimated that $1.205(5) \lesssim g_{c2} \lesssim 1.390(2)$.

$1.205(5) \lesssim g_{c2} \lesssim 1.390(2)$; see Fig. 8. However, there is no transition of phases nearby. There are two possibilities: one being that our POVM for $g > 1$ is not optimal but the quantum computational power extends further beyond, or it is possible that the quantum computational power does not extend all the way to the whole SPT phase. However, we do not have the means to resolve this. Obtaining a whole SPT phase that provides universal resource for quantum computation will likely further strengthen the connection between quantum computation and the SPT order in two and higher dimensions. Such connection and whether quantum computa-
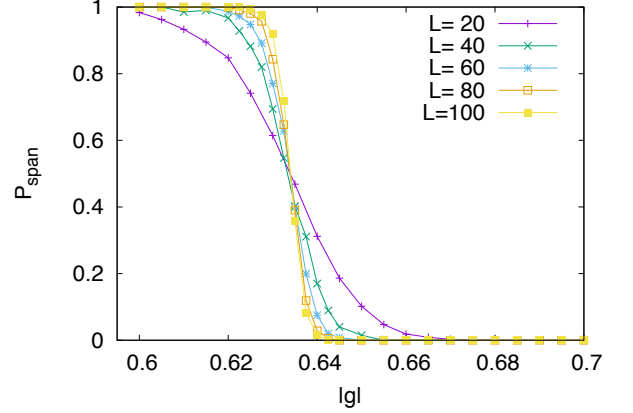
FIG. 9. Probability P_{span} of a spanning loop (i.e. a macroscopic GHZ loop) vs. parameter g for the case $g < 1$ for various linear sizes L on the square lattice. The total number of squares is L^2. A percolation transition is estimated at $g_{c1} \approx 0.635(3)$ in the thermodynamic limit. In the region $g_{c1} < g \leq 1$, there is no macroscopic GHZ loop ($P_{\text{span}} \to 0$ as $L \to \infty$) and hence a sufficiently large valence-bond state with the number of qubits being proportional to the original system size can be obtained. This means that the system provides a universal resource for MBQC.

tional capability extends to the whole SPT phase may also depend on the SPT order. Characterizing such a connection would certainly reveal the fundamental connection of quantum computational power and topological symmetric phases of matter.

Appendix E: Square lattice

Here we present the construction of the POVM, the outcome probability and the simulation results for the square lattice.

1. POVM outcome probability for $|g| \leq 1$

Since the phase is local to each site of three qubits, for the purpose of quantum computation we can transform it away by local unitary. Thus, for simplicity, we only need to consider $g > 0$ case. In this part we first discuss the parameter range $0 \leq g \leq 1$. In this region, we construct a local POVM that contains two elements $\{E_1 = F_1^\dagger F_1, E_2 = F_2^\dagger F_2\}$, where

$$F_1 = g(|0000\rangle\langle 0000| + |1111\rangle\langle 1111|) + \sum_{\text{rest}} |\text{rest}\rangle\langle\text{rest}|$$

$$F_2 = \sqrt{1 - g^2}(|0000\rangle\langle 0000| + |1111\rangle\langle 1111|), \qquad \text{(E1)}$$

where $|\text{rest}\rangle\langle\text{rest}|$ denotes product projectors other than those associated with 0000 and 1111. One can verify that

$E_1 + E_2 = \mathbb{1}$ and thus the POVM is trace-preserving. The argument used in the honeycomb case can be repeated to show that the probability of a particular outcome $\{\alpha_v\}$ is proportiontal to

$$P_{\{\alpha_v\}} = p_0 \, g^{2n_1} (1 - g^2)^{n_2} \, 2^{\sum_c (1 - |c|)}, \qquad \text{(E2)}$$

where p_0 is an overall constant that is independent of $\{\alpha_v\}$.

Using this we have performed Monte Carlo simulations and obtain the quantum computational universality disappears at $g_c \approx 0.635(3)$ when g decreases from 1; Fig. 9.

2. Case $|g| > 1$

In this region of the parameter, we consider a different POVM that contains two elements $\{E_3 = F_3^\dagger F_3, E_4 = F_4^\dagger F_4\}$, where

$$F_3 = \frac{1}{g} \sum_{\text{rest}} |\text{rest}\rangle\langle\text{rest}| + |0000\rangle\langle0000| + |1111\rangle\langle1111|$$

$$F_4 = \frac{\sqrt{g^2 - 1}}{g} \sum_{\text{rest}} |\text{rest}\rangle\langle\text{rest}|. \qquad \text{(E3)}$$

One can verify that $E_3 + E_4 = \mathbb{1}$ and thus the POVM is trace-preserving. Similar to the honeycomb case, the probability of a particular outcome $\{\alpha_v\}$ can be shown to be

$$P_{\{\alpha_v\}} = p_0' \, g^{-2n_3} \left(\frac{g^2 - 1}{g^2} \right)^{-n_4} \prod_c q_c \, 2^{-|c|}, \qquad \text{(E4)}$$

where p_0' is an overall constant that is independent of $\{\alpha_v\}$, and q_c counts the number of components in the merged generalized GHZ state for the cluster c. Since the there are four partons on a site, the q_c has slightly different bounds: $14 \le q_c \le 14^{|c|/4}$.

Using this we have performed Monte Carlo simulations and obtain the quantum computational universality disappears at g_{c2}, where $1.31(1) \lesssim g_{c2} \lesssim 1.82(1)$.

[1] P. W. Shor, Algorithms for quantum computation: Discrete logarithms and factoring, Proc. 35nd Annual Symposium on Foundations of Computer Science (Shafi Goldwasser, ed.), IEEE Computer Society Press (1994), 124-134.

[2] L. Grover, A fast quantum mechanical algorithm for database search, in Proceedings of the 28th Annual ACM Symposium on the Theory of Computation (New York, 1996) ACM, 212-219.

[3] A. M. Childs, R. Cleve, E. Deotto, E. Farhi, S. Gutmann, and D. A. Spielman, Exponential algorithmic speedup by quantum walk, in Proceedings of the 35th ACM Symposium on Theory of Computing (2003), 5968.

[4] S. Hallgren, Polynomial-time quantum algorithms for Pells equation and the principal ideal problem, Journal of the ACM **54** (1): Art. No. 4 (2007).

[5] A. W. Harrow, A. Hassidim, and S. Lloyd, Quantum Algorithm for Linear Systems of Equations, Phys. Rev. Lett. **103**, 150502 (2009).

[6] D. Bacon and W. van Dam, Recent Progress in Quantum Algorithms, Communications of the ACM, **53**, pp. 84-93 (2010).

[7] D. Nagaj, R. D. Somma, and M. Kieferova, Quantum Speedup by Quantum Annealing, Phys. Rev. Lett. **109**, 050501 (2012).

[8] S. Cottrell and M. Hillery, Finding Structural Anomalies in Star Graphs Using Quantum Walks, Phys. Rev. Lett. **112**, 030501 (2014).

[9] P. J. Love, An efficient quantum algorithm for the Moebius function, arXiv:1412.3817 (2014).

[10] M. Nielsen and I. Chuang, Quantum Computation and Quantum Information (Cambridge University Press, Cambridge, UK, 2000).

[11] C. Nayak, S. H. Simon, A. Stern, M. Freedman, and S. Das Sarma, Non-Abelian anyons and topological quantum computation, Rev. Mod. Phys. **80**, 1083 (2008).

[12] E. Farhi, J. Goldstone, S. Gutmann, J. Lapan, A. Lundgren, and D. Preda, A quantum adiabatic evolution algorithm applied to random instances of an NP-complete problem, Science **292**, 472 (2001).

[13] D. Averin, Adiabatic quantum computation with Cooper pairs, Solid State Comm. **105**, 659 (1998).

[14] A. M. Childs, Universal Computation by Quantum Walk, Phys. Rev. Lett. **102**, 180501 (2009).

[15] H. J. Briegel, D. E. Browne, W. D′ur, R. Raussendorf, and M. Van den Nest, Measurement-based quantum computation, Nat. Phys. **5**, 19 (2009).

[16] R. Raussendorf and T.-C. Wei, Quantum Computation by Local Measurement, Annu. Rev. Condens. Matter Phys. **3**, 239 (2012).

[17] L. C. Kwek, Z. H. Wei, and B. Zeng. Measurement-Based Quantum Computing with Valence-Bond-Solids, Int. J. Mod. Phys. B **26**, 123002 (2012).

[18] D. Gottesman and I. L. Chuang, Demonstrating the viability of universal quantum computation using teleportation and single-qubit operations, Nature **402**, 390 (1999).

[19] F. Verstraete and J. I. Cirac, Valence-bond states for quantum computation, Phys. Rev. A **70** 060302(R) (2004).

[20] R. Raussendorf and H. J. Briegel, A One-Way Quantum Computer, Phys. Rev. Lett. **86**, 5188 (2001).

[21] R. Raussendorf, D. E. Browne, and H. J. Briegel, Measurement-based quantum computation using cluster states, Phys. Rev. A **68**, 022312 (2003).

[22] P. Aliferis and D. W. Leung, Computation by measurements: A unifying picture, Phys. Rev. A **70**, 062314 (2004).

[23] M. Van den Nest, W. Dür, G. Vidal, and H. J. Briegel,

Classical simulation versus universality in measurement-based quantum computation, Phys. Rev. A **75**, 012337 (2007).

[24] M. Van den Nest, W. Dür, A. Miyake, and H. J. Briegel, Fundamentals of universality in one-way quantum computation, New J. Phys. **9**, 204 (2007).

[25] D. Gross, S. T. Flammia, and J. Eisert, Fundamentals of universality in one-way quantum computation, Phys. Rev. Lett. **102**, 190501 (2009).

[26] M. J. Bremner, C. Mora, and A. Winter, Are Random Pure States Useful for Quantum Computation? Phys. Rev. Lett. **102**, 190502 (2009).

[27] Z.-C. Gu, and X.-G. Wen, Tensor-entanglement-filtering renormalization approach and symmetry protected topological order Phys. Rev. B **80** 155131 (2009).

[28] X. Chen, Z.-C. Gu, and X.-G. Wen, Complete classification of 1D gapped quantum phases in interacting spin systems, Phys. Rev. B **84**, 235128 (2011).

[29] F. Pollmann, E. Berg, A. M. Turner, and M. Oshikawa, Symmetry protection of topological order in one-dimensional quantum spin systems , Phys. Rev. B **85**, 075125 (2012).

[30] N. Schuch, D. Pérez-García, and I. Cirac, Classifying quantum phases using MPS and PEPS, Phys. Rev. B **84**, 165139 (2011).

[31] X. Chen, Z.-C. Gu, Z.-X. Liu, and X.-G. Wen, Symmetry-Protected Topological Orders in Interacting Bosonic Systems, Science **338**, 1604 (2012).

[32] X. Chen, Z.-C. Gu, Z.-X. Liu, and X.-G. Wen, Symmetry protected topological orders and the group cohomology of their symmetry group, Phys. Rev. B **87**, 155114 (2013).

[33] D. V. Else, I. Schwarz, S. D. Bartlett, and A. C. Doherty, Symmetry-Protected Phases for Measurement-Based Quantum Computation, Phys. Rev. Lett. **108**, 240505 (2012).

[34] D. Gross and J. Eisert, Novel Schemes for Measurement-Based Quantum Computation, Phys. Rev. Lett. **98**, 220503 (2007).

[35] G. K. Brennen and A. Miyake, Measurement-Based Quantum Computer in the Gapped Ground State of a Two-Body Hamiltonian, Phys. Rev. Lett. **101**, 010502 (2008).

[36] A. Prakash and T.-C. Wei, Ground-state forms of 1D symmetry-protected topological phases and their utility as resource states for measurement-based quantum computation, Phys. Rev. A **92**, 022310 (2015).

[37] J. Miller and A. Miyake, Resource Quality of a Symmetry-Protected Topologically Ordered Phase for Quantum Computation, Phys. Rev. Lett. **114**, 120506 (2015).

[38] D. T. Stephen, D.-S. Wang, A. Prakash, T.-C. Wei, and R. Raussendorf, Determining the computational power of symmetry protected topological phases, Phys. Rev. Lett. **119**, 010504 (2017).

[39] R. Raussendorf, D.-S. Wang, A. Prakash, T.-C. Wei, and D. Stephen, Symmetry-protected topological phases with uniform computational power in one dimension, Phys. Rev. A **96**, 012302 (2017).

[40] H. Poulsen Nautrup and T.-C. Wei, Symmetry-protected topologically ordered states for universal quantum computation, Phys. Rev. A **92**, 052309 (2015).

[41] J. Miller and A. Miyake, Hierarchy of universal entanglement in 2D measurement-based quantum computation, NPJ Quantum Information **2**, 16036 (2016).

[42] J. Miller and A. Miyake, Latent Computational Complexity of Symmetry-Protected Topological Order with Fractional Symmetry, arXiv:1612.08135 (2016).

[43] X. Chen, Z.-X. Liu, and X.-G. Wen, Two-dimensional symmetry-protected topological orders and their protected gapless edge excitations, Phys. Rev. B **84**, 235141 (2011).

[44] C.-Y. Huang and T.-C. Wei, Detecting and identifying 2D symmetry-protected topological, symmetry-breaking and intrinsic topological phases with modular matrices via tensor-network methods, Phys. Rev. B **93**, 155163 (2016).

[45] M. Levin and Z.-C. Gu, Braiding statistics approach to symmetry-protected topological phases, Phys. Rev. B **86**, 115109 (2012).

[46] L.-Y. Hung and X.-G. Wen, Universal symmetry-protected topological invariants for symmetry-protected topological states, Phys. Rev. B **89**, 075121 (2014).

[47] T.-C. Wei, I. Affleck, and R. Raussendorf, Affleck-Kennedy-Lieb-Tasaki State on a Honeycomb Lattice is a Universal Quantum Computational Resource, Phys. Rev. Lett. **106**, 070501 (2011).

[48] A. Miyake, Quantum computational capability of a two-dimensional valence bond solid phase, Ann. Phys. (Leipzig) **326**, 1656 (2011).

[49] T.-C. Wei, I. Affleck, and R. Raussendorf, Two-dimensional Affleck-Kennedy-Lieb-Tasaki state on the honeycomb lattice is a universal resource for quantum computation, Phys. Rev. A **86**, 032328 (2012).

[50] T.-C. Wei, Quantum computational universality of spin-3/2 Affleck-Kennedy-Lieb-Tasaki states beyond the honeycomb lattice, Phys. Rev. A **88**, 062307 (2013).

[51] T.-C. Wei, P. Haghnegahdar, R. Raussendorf, Hybrid valence-bond states for universal quantum computation, Phys. Rev. A **90**, 042333, (2014).

[52] T.-C. Wei and R. Raussendorf, Universal measurement-based quantum computation with spin-2 Affleck-Kennedy-Lieb-Tasaki states, Phys. Rev A **92**, 012310 (2015).

[53] A. S. Darmawan, G. K. Brennen, and S. D. Bartlett, Measurement-based quantum computation in a 2D phase of matter, New J. Physics, **14**, 013023 (2012).

[54] A. S. Darmawan and S. D. Bartlett, Graph states as ground states of two-body frustration-free Hamiltonians, New J. Phys. **16**, 073013 (2014).

[55] C.-Y. Huang, M. A. Wagner, and T.-C. Wei, Emergence of the XY-like phase in the deformed spin-3/2 AKLT systems, Phys. Rev. B **94**, 165130 (2016).